Temperature and Halide Dependence of the Photocycle of Halorhodopsin from *Natronobacterium pharaonis*

Igor Chizhov and Martin Engelhard
Max-Planck-Institut für Molekulare Physiologie, 44227 Dortmund, Germany

ABSTRACT The photocycle kinetics of halorhodopsin from *Natronobacterium pharaonis* (pHR_{575}) was analyzed at different temperatures and chloride concentrations as well as various halides. Over the whole range of modified parameters the kinetics can be adequately modeled with six apparent rate constants. Assuming a model in which the observed rates are assigned to irreversible transitions of a single relaxation chain, six kinetically distinguishable states (P_{1-6}) are discernible that are formed from four chromophore states (spectral archetypes S_i: K_{570}, $L(N)_{520}$, O_{600}, pHR'_{575}). Whereas P_1 coincides with K_{570} (S_1), both P_2 and P_3 have identical spectra resembling L_{520} (S_2), thus representing a true spectral silent transition between them. P_4 constitutes a fast temperature-dependent equilibrium between the chromophore states S_2 and S_3 (L_{520} and O_{600}, respectively). The subsequent equilibrium (P_5) of the same spectral archetypes is only moderately temperature dependent but shows sensitivity toward the type of anion and the chloride concentration. Therefore, S_2 and S_3 occurring in P_4 as well as in P_5 have to be distinguished and are assigned to $L_{520} \leftrightarrow O^1_{600}$ and $O^2_{600} \leftrightarrow N_{520}$ equilibrium, respectively. It is proposed that P_4 and P_5 represent the anion release and uptake steps. Based on the experimental data affinities of the halide binding sites are estimated.

INTRODUCTION

The four archaeal rhodopsins discovered in *Halobacterium salinarum* are involved in phototaxis and energy conversion. The two sensory rhodopsins SRI and SRII mediate the locomotive response of the bacteria to altered light conditions (reviewed by Hoff et al., 1997; Schäfer et al., 1999) directing them to environments in which the two light-driven ion pumps halorhodopsin (HR) and bacteriorhodopsin (BR) are activated. In this way a membrane potential is generated that enables the bacteria to support energy-requiring steps and even to grow under low oxygen supply (Hartmann and Oesterhelt, 1977; Michel and Oesterhelt, 1980; Wittenberg, 1995).

Halorhodopsin (reviewed in Oesterhelt, 1995; Lanyi and Váró, 1995) was first described and named by Mukohata and co-workers (Matsuno-Yagi and Mukohata, 1980). In subsequent work, HR was recognized as an inward-directed chloride pump (Schobert and Lanyi, 1982), and the amino acid sequence had been determined (Blanck and Oesterhelt, 1987). The primary structure revealed considerable sequence identities between BR and HR. However, notable differences are connected with the ion uptake and release pathways in which aspartic acids are substituted by neutral residues. In BR, Asp85, which accepts the proton from the Schiff base during the photoreaction cycle (photocycle), is replaced in HR by a Thr, creating a halide-binding site. Indeed, mutating this site from Asp to Thr turns BR into a chloride pump (Sasaki et al., 1995). The other amino acid, Asp96, of BR (the proton donor to the Schiff base) is altered in HR to an Ala residue.

The isomeric state of the retinal chromophore in dark- and light-adapted HR from the bacterial species *Halobacterium salinarum* (sHR) and *Natronobacterium pharaonis* (pHR) has recently been re-measured by FT-Raman spectroscopy and retinal extraction experiments (Zimányi and Lanyi, 1997). The dark-adapted sample of sHR contains ~55% of the 13-*cis* isomer, whereas in the light-adapted sample 75% all-*trans* retinal accumulates (from extraction experiments a value of 83% was determined). In contrast to the latter result a light/dark adaptation has not been found in pHR. Both the light- and dark-adapted state contained ~85% all-*trans* retinal. A similar result was obtained by Gerscher et al. (1997). Zimányi and Lanyi (1997) noticed that the transient absorption changes of pHR corresponded to those of sHR after subtraction of the contribution of the 13-*cis* components.

A projection map of sHR with at a resolution of 6 Å has been published (Havelka et al., 1993). More recently the crystallographic structure of the sHR at 1.8-Å resolution showed striking similarities to that of BR (Kolbe et al., 2000). Interestingly, the chloride-binding site comprises, besides the protonated Schiff base, two water molecules and OH of Ser115 as well as the hydrophobic methyl group of Thr 111.

The photocycle of sHR has been studied in great detail (Tsuda et al., 1982; Taylor et al., 1983; Hegemann et al., 1985; Oesterhelt et al., 1985; Lanyi and Vodyanoy, 1986; Tittor et al., 1987; Zimányi et al., 1989; Váró et al., 1995a). In more recent years, pHR became available (Bivin and Stoeckenius, 1986; Lanyi et al., 1990; Scharf and Engelhard, 1994), whose photocycle and transport properties have been the focus in a number of publications (Duschl et al., 1990; Váró et al., 1995b,c; Gerscher et al., 1997; Kalaid-

Received for publication 29 December 2000 and in final form 8 June 2001.
Address reprint requests to Dr. Igor Chizhov, Max-Planck-Institut für Molekulare Physiologie, Otto-Hahn Strasse 11, 44227 Dortmund, Germany. Tel.: 49-231-1332376; Fax: 49-231-1332699; E-mail: chizhov@mpi-dortmund.mpg.de.

0006-3495/01/09/1600/13 $2.00

zidis et al., 1998; Muneyuki et al., 1999; Okuno et al., 1999; Ludmann et al., 2000). The results emerging from these investigations display a photocycle that has close resemblance to that of sHR. Archetypal intermediates are named K, L, N, and O in analogy to those described for BR. Additionally, a species appearing late in the photocycle has been identified (HR′) whose spectroscopic properties are quite similar to those of the basis state (Váró et al., 1995b). Originally, it had been introduced (as $^{T}HR_x$) into the HR photocycle by Ames et al. (1992) on the ground of their C-T model.

From kinetic studies on sHR as well as pHR a photocycle scheme was proposed that includes a spectrally silent transition between L_1 and L_2 (Ames et al., 1992; Oesterhelt, 1995; Váró et al., 1995a; Ludmann et al., 2000) and follows a linear sequence of intermediates: $K\leftrightarrow L_1\leftrightarrow L_2\leftrightarrow N\leftrightarrow O\leftrightarrow HR'\rightarrow HR$ (Ludmann et al., 2000). The photocycles of sHR and pHR are distinguished from each other by the appearance of the O-intermediate, which does not accumulate in the all-*trans* photocycle of sHR (Váró et al., 1995a).

The electrogenic activity of sHR has been elucidated early on using different approaches. The function of HR as an inward-directed chloride pump was first established by Schobert and Lanyi (1982). In subsequent work, sHR was reconstituted into black lipid membranes, and it could be demonstrated that not only chloride is pumped but also bromide and iodide (Bamberg et al., 1984). The photoresponse occurs with half-saturation concentrations in the order of 1–10 mM. Interestingly, the authors note that the photocurrent is inhibited at higher bromide or iodide concentrations. This observation has been further substantiated in recent work (Okuno et al., 1999).

Time-resolved measurements of the electrogenic steps in the photocycle of pHR revealed that chloride release and uptake are closely related to the formation and decay of the O-intermediate (Bamberg et al., 1993; Váró et al., 1995c; Kalaidzidis et al., 1998; Ludmann et al., 2000). Conceptually, the chloride uptake and release must be separated either via kinetic competition or via conformational regulation to obtain a vectorial transport. A model based on the former possibility was put forward by Lanyi (1999) in his local access model, whereas the latter option is fulfilled in the isomerization-switch-transport (IST) model of Haupts et al. (1997). However, one should keep in mind that also the fine tuning of both thermodynamic and kinetic parameters (e.g., ΔG and $\Delta G^{\ddagger}$) might be responsible for the efficient ion transport in bacterial rhodopsins.

To gain a deeper insight into the mechanism of the ion transport in halorhodopsin the photocycle of pHR in dependence of temperature, chloride concentration, and type of anion is analyzed. The results indicate that two O-intermediates (O^1_{600} and O^2_{600}) are formed that might play the same role in HR as M_1 and M_2 in the mechanism of the proton transport in the BR photocycle (reviewed by Lanyi, 1999).

MATERIALS AND METHODS

Sample purification and preparation

Pharaonis halorhodopsin was isolated from *N. pharaonis* as described elsewhere (Scharf and Engelhard, 1994). For the flash photolysis experiments, pHR (OD ~1) was solubilized in 10 mM citrate/phosphate buffer (pH 6.0) containing 0.1% dodecyl maltoside (DM) and appropriate amounts of NaCl, NaBr, or NaI. The ionic strength of the solutions were kept constant equivalent to the 2 M monovalent salt by addition of Na_2SO_4 (e.g., 0.15 M NaCl + 0.62 M Na_2SO_4 ∝ 2 M NaCl).

Photocycle measurements

The laser flash photolysis setup was similar to that described by Chizhov and co-workers (Chizhov et al., 1996, 1998). Two digital oscilloscopes (LeCroy 9361 and 9400A, 25 and 32 kilobytes of buffer memory per channel, respectively) were used to record the traces in two overlapping time windows. The maximal digitizing rate was 10 ns per data point. Transient absorption changes were recorded from 10 ns after the laser pulse (Nd:YAG, 532 nm, 10 ns, 5 mJ/cm^2) until full completion of the photocycle. At each wavelength, 25 laser pulses were averaged to improve the signal-to-noise ratio. The quasi-logarithmic data compression reduced the initial number of data points per trace (~50,000) to ~600 points evenly distributed in log time scale giving ~100 points per time decade. The correspondent improvement of signal-to-noise ratio was accounted for by the data weights that were initially estimated from the noise of the pretrigger base line. Excluding data points up to 200 ns after the laser pulse cut off the laser artifact at early times. The wavelengths were varied from 400 to 710 nm in steps of 10 nm (altogether, 32 spectral points; the step size was reduced to 5 nm for the 150 mM NaCl, NaBr, and NaI preparations at 20°C (63 wavelengths per data set)). Absorption spectra of the samples were measured before and after each experiment. The latter provides a control for the absence of irreversible photobleaching of the chromophore.

Three external parameters were varied: 1) the temperature in 5°C steps from 0°C to 50°C (150 mM NaCl, 11 data sets), 2) NaCl concentration (from 150 mM to 2 M, 20°C, 5 data sets), and 3) the type of halide anion (150 mM chloride, bromide, and iodide, 20°C, 3 data sets). The resulting 19 data sets were used for the analysis.

Data analysis

Each data set was independently analyzed using the global multi-exponential nonlinear least-squares fitting program MEXFIT (Müller et al., 1991; Müller and Plesser, 1991). The number of exponential components was incremented until the standard deviation of weighted residuals did not further improve. Additionally, the randomness of the three-dimensional surface of weighted residuals and the smoothness of the temperature dependence of the derived rate constants and their amplitude spectra were used to determine the number of exponents.

After establishing the apparent rate constants and their assignment to the internal irreversible transitions of a single chain of relaxation, the amplitude spectra of exponents were transformed to the differential spectra of the corresponding intermediates. Subsequently, the absolute absorption spectra of states were determined by adding the differential spectra divided by the fraction of cycling to the spectra of the initial states. Criteria for the determination of the fraction cycling were the absence of negative absorbencies and contributions from the ground state to the calculated spectra. For further details of the methods see Chizhov et al. (1998, 1996).

Finally, all derived absolute spectra were approximated by a global multi-Gaussian fit using a user-defined nonlinear least-squares fitting of the Origin 6.0 program (Microcal Software) and Igor Pro 3.16 (WaveMetrics). A skewed Gaussian function has been used to fit spectral bands

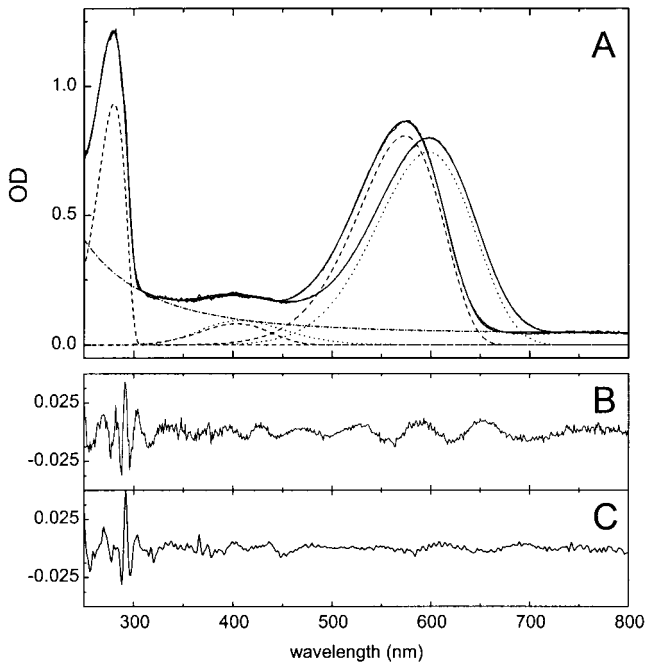

FIGURE 1 Spectra of pHR (20°C, pH 6.0, 0.15 M NaCl, 0.62 M Na_2SO_4) and pHR_{blue} (20°C, pH 6.0, 0.67 M Na_2SO_4) and their Gaussian fit consisting of three components. (*A*) Spectra of pHR and pHR_{blue} and their fits (——); components S_{01}, S_{02} and S_{03} (S_{03}^{blue}) (- - - -); S_{01}^{blue} and S_{02}^{blue} (· · ·); and light-scattering fit (– · –). (*B* and *C*) The residuals plots: phR minus fit (*B*) and phR_{blue} minus fit (*C*). All parameters of the fitting are summarized in Table 1.

(Birge, 1990, Chizhov et al., 1996, 1998; see last two references for the analytical form applied here).

RESULTS

Multi-Gaussian fit of the absorption spectra of pHR

Three skewed Gaussian functions S_{01}, S_{02}, and S_{03} as well as a function describing the Rayleigh scattering approximate the pHR and pHR_{blue} ground spectra (see Fig. 1 *A*). The residuals for the pHR and pHR_{blue} are plotted in Fig. 1, *B* and *C*, respectively. The fitted parameters are given in Table 1, where ρ is a parameter of skewness that is an indirect measure of the Frank-Condon effect. It represents an asymmetry of the Gaussian function, e.g., $\Delta\nu = \Delta\nu_L + \Delta\nu_R = (1 + \rho)\Delta\nu_L$, where $\Delta\nu$ is the half-bandwidth, and $\Delta\nu_L$ is a low-energy component of $\Delta\nu$ (width from the left of the maximum in cm^{-1}).

The amplitudes of components are normalized to the band at 574 nm (S_{01}). The background scattering line has been fitted by $A + B/\lambda^C$ (λ in nm) with $A = 0.041 \pm 0.001$, $B = (5.9 \pm 6.8) \times 10^8$, and $C = 3.8 \pm 0.2$. The A_{280}/A_{575} ratio is 1.16, slightly lower than that previously reported of 1.4 (Duschl et al., 1990). The pronounced systematic deviations of residuals in the UV region indicate the necessity to fit Trp and Tyr aromatic residues separately. The absorption spectrum of pHR depends slightly on the temperature. At 0°C the maximum shifts to 576 nm and the amplitude increases by ~2%, and at 50°C it shifts to 573 nm and decreases by 3% with respect to the spectrum at 20°C. These variations were too small to be studied systematically. Thus, the pHR and pHR_{blue} spectra parameters in Table 1 refer to 20°C. Note that the derived spectra of four chromophore states of the photocycle given in Table 1 (S_{1-4}) and described below do not show a temperature dependence higher than that of the ground-state spectrum. Thus, within the measured temperature range all analyzed spectra should be considered as highly temperature insensitive.

TABLE 1 Parameters of the Gaussian fit of spectral states of the pHR

	A_{max}, OD	ρ	$\Delta\nu$ (cm^{-1})	λ_{max} (nm)
$S_{01}/(S_4)$	1.0 ± 0.003	1.60 ± 0.01	3200 ± 10	574 ± 0.1
S_{02}	0.1 ± 0.003	1.42 ± 0.08	5200 ± 220	404 ± 1
S_{03}	1.16 ± 0.004	1.86 ± 0.02	4750 ± 55	280 ± 0.1
SD = 7 mOD				
S_{01}^{blue}	0.92 ± 0.003	1.46 ± 0.01	3350 ± 10	598 ± 0.1
S_{02}^{blue}	0.12 ± 0.003	1.1 ± 0.05	6020 ± 150	407 ± 1
S_{03}^{blue}	1.16 ± 0.003	1.9 ± 0.02	4800 ± 50	280 ± 0.07
SD = 5 mOD				
$S_1(K)$	0.86 ± 0.02	1.40 ± 0.01	3400 ± 15	571 ± 0.3
SD_{11} = 22 mOD				
$S_2(L,N)$	0.62 ± 0.02	1.43 ± 0.02	3450 ± 20	521 ± 0.2
$S_3(O)$	0.7 ± 0.03	1.60 ± 0.03	3700 ± 50	597 ± 0.5
SD_{60} = 10 moD				

The transition from the pHR_{blue} to pHR occurs upon an addition of halide anions in the millimolar range. The apparent K_d of chloride, bromide (Scharf and Engelhard, 1994), and iodide (data not shown) binding to pHR_{blue} is 2.5, 1, and 3 mM, respectively. At the halide concentrations higher than 150 mM where the photocycle kinetics were studied, the contribution of the pHR_{blue} is lower than 1%, i.e., quite below the resolution level.

Multi-exponential global analysis

Fig. 2 shows the transient absorption changes after 10-ns laser photoexcitation of the pHR (pH 6.0, 150 mM NaCl) at three characteristic wavelengths and six temperatures from 0°C to 50°C. These six data sets as well as those from the other five temperature points, the five concentrations of NaCl, and the three different anions Cl, Br, and I were fitted independently by a nonlinear multi-exponential fitting program. Through the whole range of the varied parameters it is sufficient and necessary to approximate the experimental data with six kinetic components (rate constants). The addition of a seventh rate constant does not further improve the standard deviation of weighted residuals but introduces

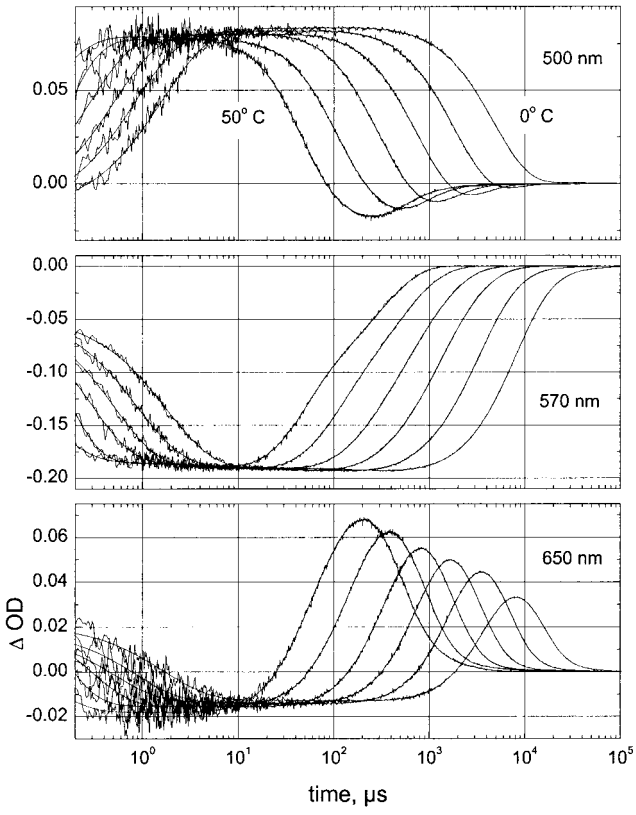

FIGURE 2 Traces of the transient absorption changes after photoexcitation of pHR at different temperatures (from 0°C to 50°C, step 10°C, pH 6.0, 0.15M NaCl, 0.62 M Na_2SO_4). The time courses are shown only for selected wavelengths (500, 570, and 650 nm). Thin solid lines represent the result of the global fit using six exponents.

a less systematic dependence of the rates and amplitudes on the varied parameters. Therefore, six rate constants and their correspondent amplitude spectra were used for the analysis of the pHR photocycle.

Rate constants versus temperature, [Cl], and halide type

The temperature dependence of the pHR kinetics is depicted in Fig. 3 *A*. All rate constants except k_4 and k_6 display a linear dependence on the reciprocal temperature. The slowest component k_6 has the smallest differential spectral amplitudes (~1–2 mOD), which has to be compared with the maximal transient ΔOD of ~200 mOD. Therefore, its dependence on temperature, chloride concentration, and type of anion (Fig. 3, *A–C*) is not very well defined. On the other hand, the fourth rate constant k_4 has a significant spectral amplitude (not shown), which allows establishing a smooth convexity of the Arrhenius plot. Below, it will be shown how this behavior is coupled to the correspondent kinetic state of the photocycle and that the convex curvature of k_4 can be fitted assuming a fast temperature-dependent equilibrium within this state.

The temperature dependence of the six rate constants (Fig. 3 *A*) resemble in many respects those of the photocycle of BR (Chizhov et al., 1996) and pSRII (Chizhov et al., 1998). Although for these proteins more rates are necessary to describe the data (eight versus six) and an M-intermediate is formed, the rate constants span a similar range of time (from ~1 μs to tens or hundreds of milliseconds) and possess similar slopes in the Arrhenius plots. The activation parameters (enthalpy $\Delta H^{\ddagger}$ and entropy $\Delta S^{\ddagger}$ of activation) obtained from the temperature dependence of the rate constants are given in Table 2.

The photocycle of pHR was measured at 20°C at five different concentrations of NaCl (from 150 mM to 2 M). The correspondent rate constants are plotted in Fig. 3 *B*. It is obvious that within the logarithmic accuracy of derived rate constants only k_2, k_4, and k_5 are slightly accelerated (1.5–2-fold) at higher NaCl concentrations. It is interesting to note that k_3 and k_4 (both of them display spectral amplitudes of opposite sign) become indistinguishable at chloride concentrations higher than 300 mM (giving the correspondent half-times of ~300 μs).

The question arises whether these two rate constants are really necessary to describe the data or whether one of them can be omitted. To clarify this point, the quality of the fit was analyzed through the whole range of varied parameters. Withdrawing one of these components (or replacing it by a single one) from the initial values of the nonlinear fit increased the standard deviation of weighted residuals to ~10% whereas an addition of a seventh component decreased the standard deviation by less than 1%. Theoretically, a degeneration of two rate constants would give non-exponential kinetics of the intermediate, i.e., $\sim kte^{-kt}$. On the other hand, for a numerical fit of the data this is not essential because any numerical calculation has a sufficiently high but finite accuracy, and therefore two close rate constants would always differ. Therefore, the pHR photocycle shows us the first interesting example where one particular state has almost identical rates of formation and decay at high chloride concentrations.

The sensitivity of the pHR photocycle toward the type of halide anion (150 mM Cl, Br, or I) is shown in Fig. 3 *C*. Again, the same six rate constants are detected. Two transitions, k_1 (two times) and k_2 (five times) are affected significantly by the anion replacement. All other steps are within experimental accuracy insensitive toward the substitution.

It is important to note that the rates derived in this work are systematically faster than those published previously by other groups, although the trends are strikingly similar (Váró et al., 1995c; Kalaidzidis et al., 1998; Muneyuki et al., 1999; Ludmann et al., 2000) also with respect to the chloride dependence (Váró et al., 1995c). The discrepancies might originate from the different sample preparation.

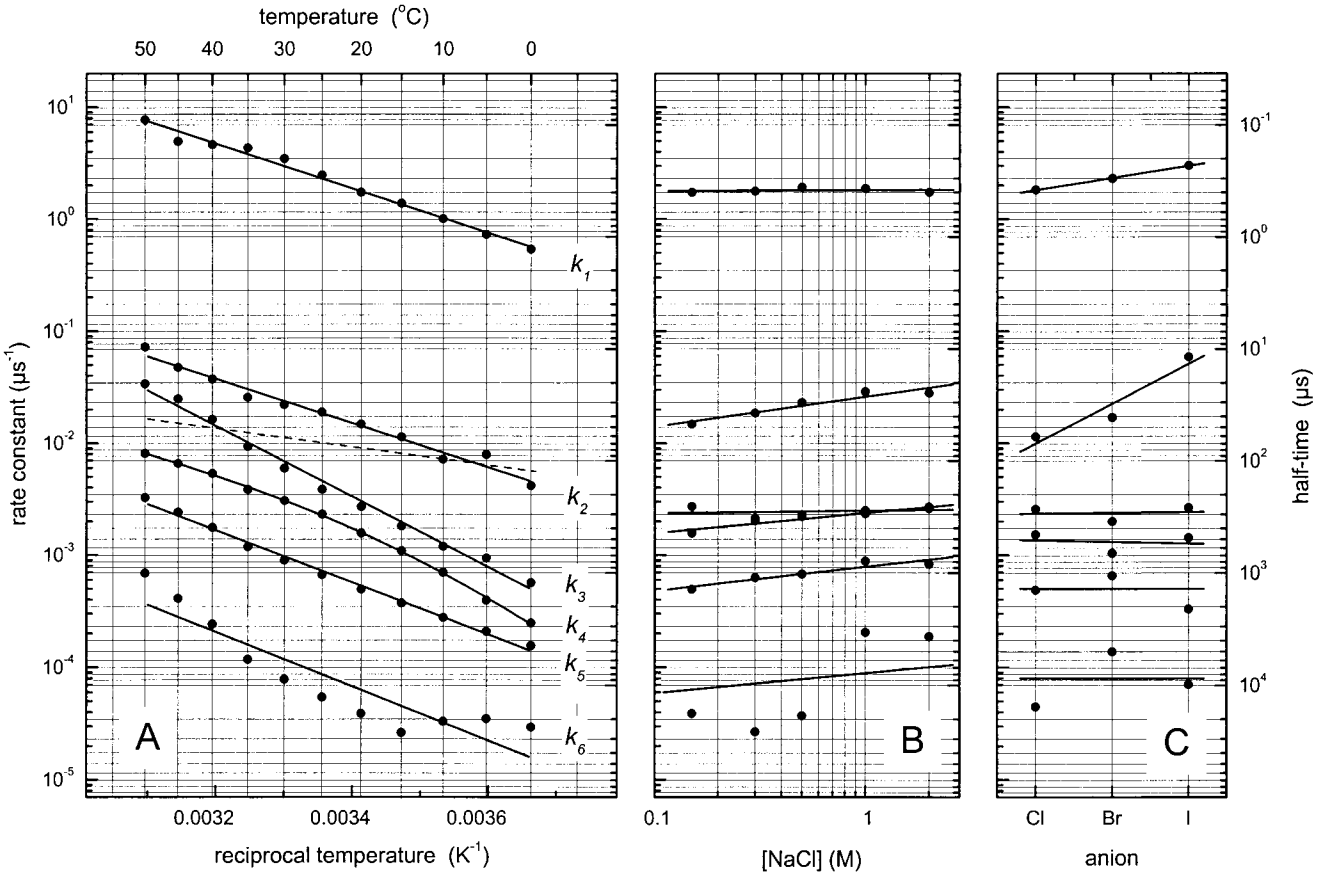

FIGURE 3 Temperature (*A*), anion concentration (*B*) and anion type (*C*) dependence of the six apparent rate constants of the pHR photocycle. The rate constants shown in the Arrhenius plot (*A*) were determined at pH 6.0, 0.15 M NaCl, 0.62 M Na_2SO_4. Straight lines in *A* represent the least-squares fit of the apparent activation parameters (see Table 2) according to the Eyring equation with exception of k_4, which has been fitted as a product of the rate (- - - -) and equilibrium (see Fig. 5) constants. Lines in *B* and *C* are drawn to guide the eye. Sample conditions were pH 6.0, 20°C, ionic strength equivalent to the 2 M monovalent salt (*B*) and pH 6.0, 20°C 150 mM of halides, 0.62 M Na_2SO_4 (*C*). The horizontal grid lines correspond to the right axis (half-times), and the vertical grid lines in *A* correspond to the top axis (°C).

Whereas in the present work pHR was isolated from the native host *N. pharaonis* the cited references describe experiments with pHR that had been heterologously expressed in *H. salinarum*. However, it should be noted that the photocycle data of pHR expressed in *Escherichia coli* are indistinguishable from those presented in this work (unpublished data).

Sequential unidirectional model

To calculate the absolute absorption spectra of states that correspond to the obtained set of the kinetic components of the photocycle the same assumption was applied that was used in the previous analysis of the photocycles of BR (Chizhov et al., 1996) and pSRII (Chizhov et al., 1998). The relaxation path is assumed as a single chain of irreversible transitions $P_1 \rightarrow P_2 \rightarrow P_3 \rightarrow P_4 \rightarrow P_5 \rightarrow P_6 \rightarrow P_0$. The general analytical solution of the corresponding system of ordinary differential equations is given by Chizhov et al. (1996). Accordingly, the absolute absorption spectra of kinetic states P_{1-6} were obtained as described in Materials and Methods. The spectra of P_i are depicted in Fig. 4 for the whole temperature range from 0°C to 50°C together with the ground spectra of the pHR (i.e., P_0 state) for comparison. The half-times correspond to the data set measured at 20°C. The dependencies of kinetic state P_5 on the chloride

TABLE 2 Apparent activation parameters of the pHR photocycle

	k_1	k_2	k_3	k_4	k_5	k_6
$\Delta H^{\ddagger}$ (kJ/mol)	36 ± 1	35 ± 2	58 ± 2	13 ± 1	42 ± 1.5	44 ± 7
$\Delta S^{\ddagger}$ (J/mol K)	−3 ± 5	−44 ± 6	20 ± 6	−124 ± 3	−49 ± 4	−61 ± 23

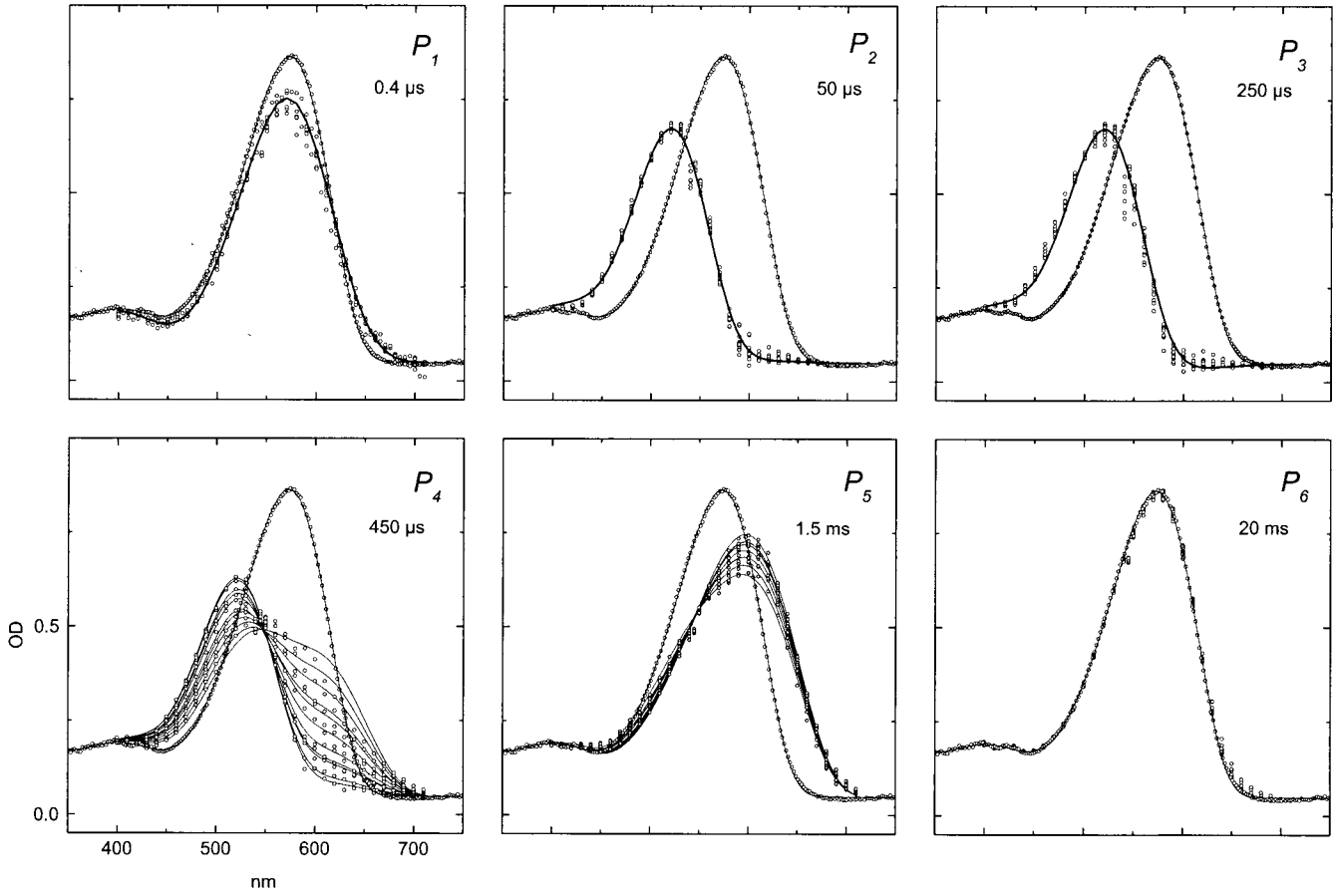

FIGURE 4 Absolute spectra of kinetic states P_1–P_6 at temperatures between 0°C and 50°C (step size 5°C, pH 6.0, 150 mM NaCl). Depicted half-times of transitions correspond to 20°C. For reasons of comparison, the initial spectrum of pHR is also shown in each panel. The figure shows the experimental data (○) and the Gaussian fit (——) of the absorption spectrum of the initial state and those of the kinetic states P_1–P_6, which were fitted globally at all measured parameters (see details in the text and Table 1 for the parameters of the fitted spectra). The spectra of the first state (P_1; K-like intermediate) could be reliably resolved only at $T \leq 25$°C. The spectra were derived from the difference spectra of the kinetic states by variation of the fraction cycling. In the whole temperature range the value of the fraction cycling is 30 ± 2%.

concentration and the type of halide anion are shown in Figs. 6 and 7, respectively. The spectra of P_i states were fitted after choosing the appropriate number of Gaussian components. Through all varied parameters we found only three spectrally distinct chromophore states, namely, S_1, S_2, and S_3, that are independent from the temperature and halide concentration. The spectrum of the last kinetic state P_6 (S_4) is almost identical to the ground pHR spectra and was therefore not fitted separately.

The spectral fittings were done globally; e.g., the spectra of the S_2 and S_3 chromophore states (Table 1) were obtained via simultaneously approximating two Gaussian bands on 60 spectra (P_2, P_3, P_4, and P_5 kinetic states at 11 temperatures and 4 additional chloride concentrations). The 6 nonlinear (2 each for ρ, $\Delta\nu$, and λ_{max}) and 120 linear (2 each for 60 amplitudes) parameters were searched using these 1920 data points. The spectra of S_1, which are present only in the P_1 state, were fitted using 11 data sets (5 temperatures (0–20°C), plus 4 concentrations, plus 2 additional halides (Br and I)). The S_2 and S_3 spectra in the presence of bromide and iodide were fitted separately (i.e., 4 data sets (P_{2-5}) for each halide) because the S_2 spectrum undergoes a systematic shift of the maximum upon halide replacement. Once no systematic dependence of the amplitudes of the component spectra upon the varied parameters was obtained, the mean value of amplitudes could be calculated. This is the case for the P_1, P_2, and P_3 kinetic states (see Fig. 4). The scattering line and β-band of the chromophore were kept constant with values from the fit of the ground spectrum of pHR (Fig. 1).

In this way, all P_i states at each temperature were approximated as shown in Figs. 4, 6, and 7 (solid lines). The correspondent Gaussian parameters of the four chromophore states $S_{j=1-4}$ together with the initial pHR spectrum that consists of three peaks (S_{01-03}) are summarized in Table 1. The spectrum of the S_4 state (see P_6 in Fig. 4) does not differ within the accuracy of the fit from the major chromophore peak of the initial state and therefore is sub-

sumed in the data of S_{01} (Table 1). In analogy to the chromophore states of the BR and pSRII photocycles these states will be named K_{570} (S_1), L_{520} or N_{520} (S_2), O_{600} (S_3), and pHR'_{575} (S_4).

Kinetic (P_i) and chromophore (S_j) states

The fastest resolved state P_1 (half-time 400 ns at 20°C) of the pHR photocycle has a temperature-independent single S_1 chromophore state with a maximum at ~570 nm and a broader half-width than the S_{01} band (3400 vs. 3200 cm^{-1}). This state resembles kinetically and spectrally the K form of the BR and pSRII photocycles although the bathochromical shift is not well established. A very similar K spectrum has been obtained by Duschl et al. (1990).

The following P_2 (50 μs) kinetic state shows also a single temperature-independent chromophore state (S_2, λ_{max} = 520 nm, $\Delta\nu = 3450$ cm^{-1}) that resembles the L form of the BR photocycle. Interestingly, the lifetime of this state is ~10 times longer than the analogous state of the BR and pSRII photocycles (Chizhov et al., 1996, 1998). The L spectra are close also to that published by Duschl et al. (1990) and Váró et al. (1995c).

The next state in the reaction sequence (P_3) has a single, temperature-independent spectrum whose properties are indistinguishable from those of P_2. Furthermore, within the experimental resolution both spectra do not alter on variation of the other parameters (NaCl concentration, anion type). Therefore, the transition from P_2 to P_3 should, with respect to its visible absorption properties, be considered as a pure spectrally silent transition.

Spectrally silent transitions can be kinetically resolved as exemplified in the following general example. In the two-step irreversible reaction A→A′→B, A and A′ are spectrally identical but differ spectrally from the final B state ($\Delta\epsilon_{AB}$). If the rate constant of A→A′ equals k_1 and that of A′→B equals k_2, the following equation applies (with A = 1 at time $t = 0$):

$$\Delta\epsilon(t) = \Delta\epsilon_{AB}\left[-\frac{k_2}{k_1 - k_2}\exp(-k_1 t) + \frac{k_1}{k_1 - k_2}\exp(-k_2 t)\right]$$

Thus, both rate constants k_1 and k_2 can be extracted from $\Delta\epsilon(t)$. In the two limiting cases, only k_2 ($k_1 \gg k_2$) or k_1 ($k_1 \ll k_2$) can be extracted. In the present example, the rate constants k_2 and k_3 of the transitions $P_2 \rightarrow P_3 \rightarrow P_4$ differ about ~5-fold; therefore, both components can be detected. The L→L′ transition is the second example of a pure spectrally silent transition in a multi-exponential relaxation sequence. An analogous transition (M→M′, ~2 ms) has been reported for the pSRII photocycle (Chizhov et al., 1998).

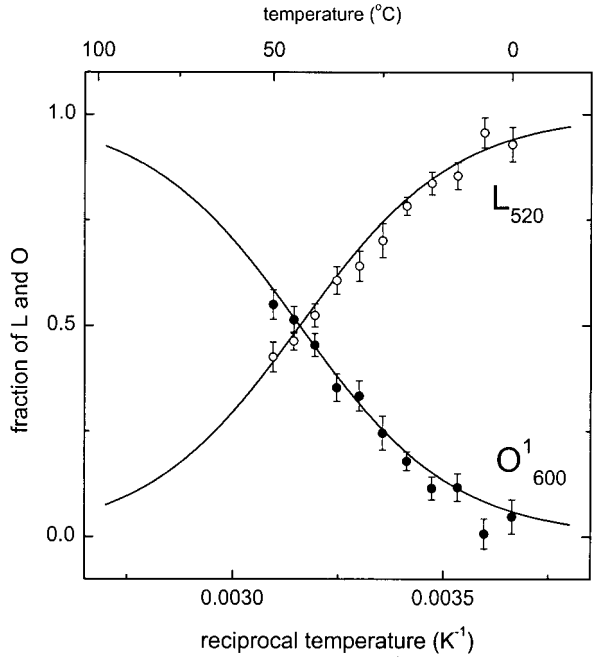

FIGURE 5 Temperature dependence of the fractions of L_{520} (○) and O^1_{600} (●) chromophore states obtained in the P_4 kinetic state. Solid lines represent the fit of data according to the thermal equilibrium equation giving the differences of enthalpy and entropy $\Delta H_{LO} = 45 \pm 5$ kJ/mol and $\Delta S_{LO} = 140 \pm 20$ J/mol K, respectively.

The next state, P_4, is characterized by a temperature-dependent equilibrium of two species (Fig. 4). At higher temperatures a component prevails that has an absorption spectrum at 600 nm. The Gaussian fit of the spectra reveals two spectral states S_2 and S_3 (Table 1). S_2, the L-like intermediate (L_{520}) has already been described above. The absorption spectrum of S_3 resembles that of the "blue" form of pHR, which is formed at a NaCl concentration below 0.1 mM NaCl and which lacks the negative counterion (chloride) of the protonated Schiff base (Scharf and Engelhard, 1994). Thus, in accordance with assignments in the literature (reviewed in Oesterhelt, 1995) the spectral features of S_3 (O_{600}) are attributed to a chloride-free Schiff base environment. Apparently, in the forward reaction of $L_{520} \leftrightarrow O^1_{600}$ at equilibrium, chloride moves away from the Schiff base and in the back reaction it is returning. We added an upper index to distinct this O state (O^1_{600}) from the chromophore state that has been found in the following kinetic state (see below). This $L_{520} \leftrightarrow O^1_{600}$ equilibrium is fast and temperature dependent.

From the Gaussian fit the relative concentrations of L_{520}(S_2) and O^1_{600} (S_3) states can be calculated that are plotted against the reciprocal temperature in Fig. 5. From this dependence, the thermodynamic parameters of the equilibrium could be determined: the chloride-free S_3 state has $\Delta H_{LO} = 45 \pm 5$ kJ/mol more enthalpy and $\Delta S_{LO} = 140 \pm 20$ J/mol K more degrees of freedom (entropy) than the S_2

state. At 293 K the gain of the free energy in the $S_2 \rightarrow S_3$ transition is 4 ± 8 kJ/mol.

These thermodynamic results can be used for the nonlinear fit of the Arrhenius dependence of k_4 (see Fig. 3 *A*), which, as discussed above, displays a characteristic curvature. Applying the corresponding equation published by Chizhov et al. (1996):

$$k_4 = \frac{kT}{h}\exp\left(-\frac{\Delta H_4^{\ddagger}}{RT} + \frac{\Delta S_4^{\ddagger}}{R}\right) \div 1 + \exp\left(\frac{\Delta H_{LO}}{RT} - \frac{\Delta S_{LO}}{R}\right),$$

the true activation barrier (dashed line in Fig. 3 *A*) of the $P_4 \rightarrow P_5$ transition is obtained. This analysis has been done under the assumption that the exit from the $S_2 \leftrightarrow S_3$ equilibrium occurs through S_3 but not S_2. The activation enthalpy $\Delta H_4^{\ddagger}$ and entropy $\Delta S_4^{\ddagger}$ values are presented in Table 2. It should be mentioned that these parameters demonstrate significant differences of the thermal activation energy as compared with the neighboring relaxation steps. The enthalpy value of a barrier is almost five times lower than those from all other transitions. Mainly the contribution of negative entropy to the barrier height moves this transition into the sub-millisecond time range.

The following kinetic state P_5 has the same two-component structure of the same spectra as P_4: S_2 (N_{520}) and S_3 (O^1_{600}) (the reasons for assigning S_2 in P_5 to an N chromophore state will be given below). However, the equilibrium is shifted in favor of S_3 (~90%) and is only moderately temperature dependent. Nevertheless, this temperature effect provided the means to calculate the relative enthalpy and entropy ΔH_{NO} = 18 ± 8 kJ/mol and ΔS_{NO} = 80 ± 30 J/mol K in favor of S_3. At 293 K these values correspond to the release of 5.4 ± 12 kJ/mol free energy in the $S_2 \rightarrow S_3$ transition.

The P_5 decays at 20°C with a half-time of 1.5 ms to the state P_6 whose spectrum (S_4) is almost identical to that of the initial state. Its half-time of ~20 ms seems to be determined by the large negative entropy of the activation barrier (see Table 2). P_6 might be considered as a precursor (pHR'_{575}) of the ground state (pHR) and k_6 as a final rearrangement of the protein, which does not affect the chromophore spectrum. Similar precursor states have also been obtained in the photocycles of BR and pSRII (Chizhov et al., 1996, 1998).

Varying the NaCl concentration at 20°C does not influence the spectra of the P_1, P_2, P_3, P_4, and P_6 kinetic states. The unique exception is the P_5 state, which shows a considerable shift of the $S_2 \leftrightarrow S_3$ equilibrium in favor of S_2 with increasing of the chloride concentration. The corresponding spectra are shown in Fig. 6. In the inset, the fractions of the S_2 (N_{520}) and S_3 (O^2_{600}) chromophore state versus concentration are shown together with a hyperbolic fit. The fit of

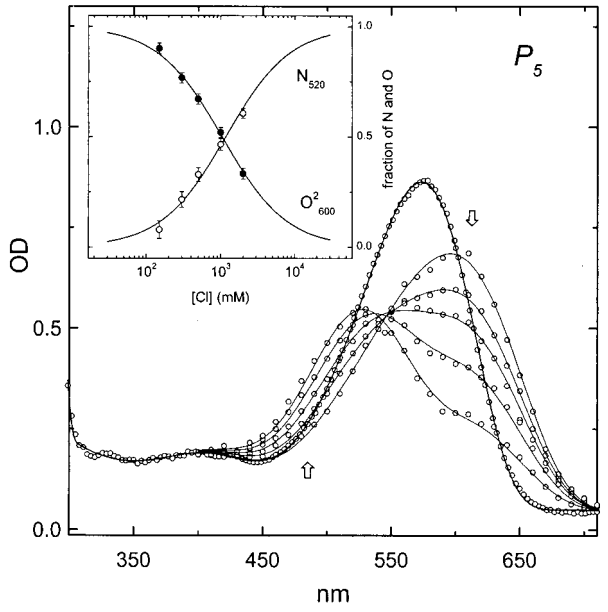

FIGURE 6 Dependence of the P_5 kinetic state on the chloride concentration. The figure shows the experimental data (○) and the Gaussian fit (——). The inset shows the fractions of N_{520} (○) and O^2_{600} (●) chromophore states obtained in P_5 versus log[Cl]. The hyperbolic fit of data (——) gives an equilibrium constant of K_d = 1.1 ± 0.2 M for chloride.

the data provided an affinity value of K_{Cl} = 1.1 ± 0.2 M. Note that at 150 mM NaCl, at which concentration the temperature dependence was measured (see above) the free energy of the S_3 state in P_5 is of $RT\ln(1.1/0.15)$ = 4.85 ± 0.4 kJ/mol lower than of the S_2 state (T = 293 K). Within the error, this is the same value as that obtained from the estimation of the temperature dependence of P_5 (5.4 ± 12 kJ/mol).

Similarly, the type of anion also has an influence on the ($S_2 \leftrightarrow S_3$) equilibrium of P_5. Upon replacement of the chloride by bromide and iodide the equilibrium is shifted in favor of S_2. The spectra are shown in Fig. 7. An absence of an isobestic point is due to spectral shifts of S_2. This trend was clearly identified on the spectra of the P_2 and P_3 kinetic states, which contain only single chromophore state S_2. The corresponding spectrum peaks shift systematically from 520 to 530 nm after replacement of chloride by bromide or iodide. The inset represents the fractions of the S_2 (N_{520}) and S_3 (O^2_{600}) chromophore state versus the type of halide. Note that 150 mM iodide or bromide induces the same shift of the equilibrium as ~2 M or 0.4 M NaCl, respectively (compare Figs. 6 and 7). This gives an estimation of affinity values of 0.3 M and 0.1 M for bromide and iodide, respectively.

The chromophore spectra of the six distinct kinetic states P_{1-6} of the photocycle and the ground pHR state have been approximated by a global Gaussian fit. They are composed of four major spectral bands S_{1-3} and $S_{01}(S_4)$. The results are shown in Fig. 8, and the corresponding parameters are

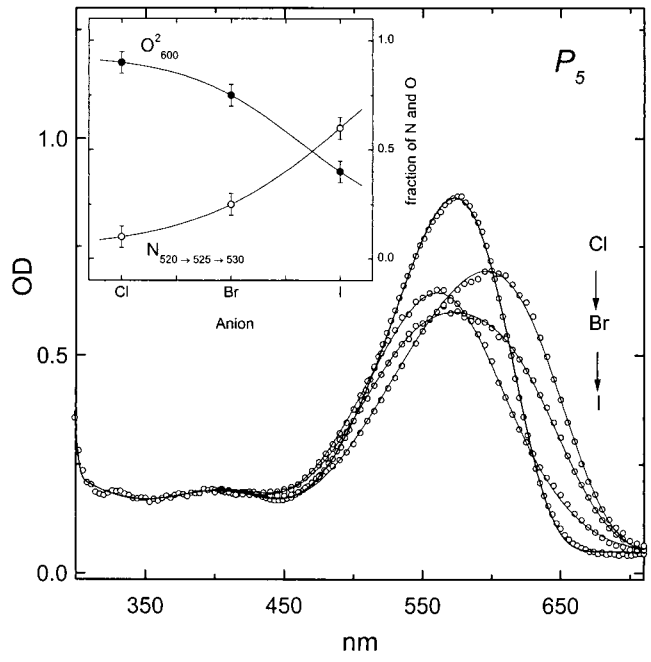

FIGURE 7 Dependence of the P_5 kinetic state on the type of halide anions. The figure shows the experimental data (○) and the Gaussian fit (——). The inset shows the fractions of N (○) and O^2_{600} (●) chromophore states versus the anion type. Note that the replacement of Cl^- by Br^- or I^- shifts the L(N) spectra from 520 to 525 or 530 nm, respectively.

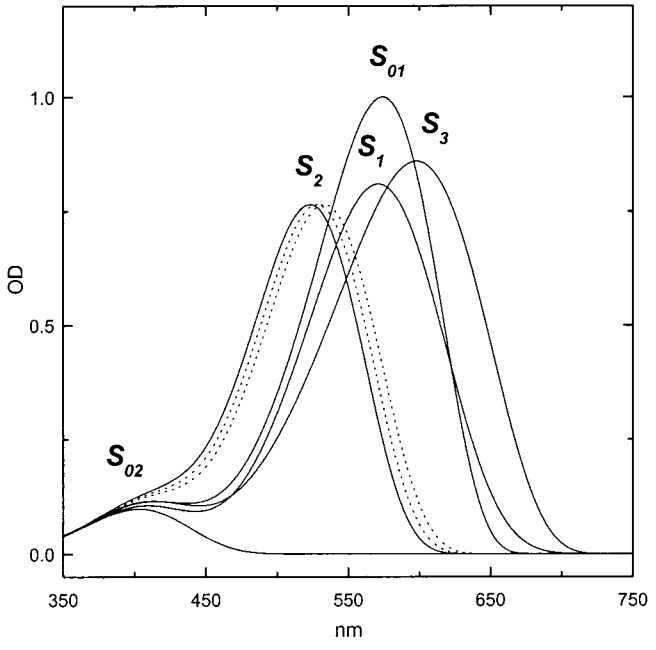

FIGURE 8 Spectra of the pHR chromophore in the initial state $S_{01,02}$, and three major archetype spectral states of the pHR photocycle S_{1-3} deduced from the global multi-Gaussian fitting of the data in Figs. 4, 6, and 7. Dotted lines are S_2 for bromide and iodide samples. The fitted parameters are compiled in Table 1.

compiled in Table 1. S_{1-3} can be assigned to the four archetypal intermediates K, (L, N), and O, respectively. These basal spectra are not altered by the external parameters, which have been applied in this work, with the exception of halide replacement. In these cases, the absorption maxima of the L and N intermediates systematically shift from 521 nm in the case of chloride as counterion to 526 nm (bromide) and 531 nm (iodide). A similar dependence for the —C═C— stretching vibration of the L intermediate has been observed in resonance Raman experiments (Gerscher et al., 1997). According to the well-known relationship between λ_{max} and the —C═C— vibration mode of retinal Schiff bases (Heyde et al., 1971), both data sets can be linearly correlated.

The $P_4 \rightarrow P_5$ transition separates two kinetic states that differ considerably in their sensitivity to external parameters. The temperature-sensitive $L_{520} \leftrightarrow O^1_{600}$ equilibrium of the P_4 state is followed by a state P_5 whose $N_{520} \leftrightarrow O^1_{600}$ equilibrium is almost insensitive toward temperature. On the other hand, the opposite sensitivity is found with respect to the NaCl concentration and the type of halide. Therefore, it can unequivocally be concluded that P_4 and P_5 are well defined kinetic states of the pHR photocycle that correspond to different stages of an anion transport. We propose that in the P_4 state the halide anion reversibly moves from the Schiff base to a second protein-binding site in the direction of the cytoplasmic surface. Conversely, the P_5 state corresponds to the reversible uptake of another anion from the extracellular medium. Thus, the reaction from P_4 to P_5 (k_4 rate constant) resembles a conformational change, which switches the accessibility of the cytoplasmic and extracellular channels as it was also proposed for the M_1-M_2 transition in BR.

DISCUSSION

The kinetic scheme of the pHR photocycle is depicted in Fig. 9. It represents eight protein transient states found in this study. Six of them are kinetically resolved (P_1 to P_6) and two are spectrally resolved as constituents of the P_4 and P_5 equilibria.

Limited by the experimental time resolution, the first transition $P_1 \rightarrow P_2$ (0.4 μs) describes already the decay of the K-intermediate. This conversion is almost identical in kinetics and relative spectral shifts to the K→L transition in BR, pSRII (Chizhov et al., 1996, 1998), or other native or mutant retinal proteins (reviewed in Oesterhelt, 1995; Lanyi and Váró, 1995). Also the Arrhenius parameters are comparable. Apparently, this transition is independent from the function or the following relaxation path of the protein and seems to be a sole feature of the photoexcitation of the protonated Schiff base.

The next two steps $P_2 \rightarrow P_3 \rightarrow P_4$ have half-times of 50 and 250 μs. They can be compared with three transitions of the BR (6, 30, and 100 μs) (Chizhov et al., 1996) and two

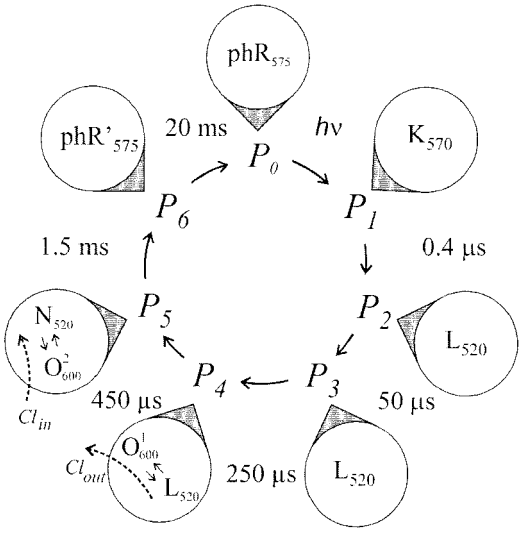

FIGURE 9 Kinetic model of the pHR photocycle. The inner circle denotes the kinetic states P_{1-6} that are further characterized by their composition of the archetypal spectral states. P_4 and P_5 represent the states in which the halides are released and taken up, respectively. The half-times are given between the circles and refer to 20°C.

transitions of the pSRII photocycle (10 and 30 μs) (Chizhov et al., 1998), which occur in the same time range. Although the kinetics and thermodynamics of the steps are comparable, the spectral changes of the intermediates in the pHR photocycle differ characteristically from those observed for BR and pSRII. In the latter photocycles these steps correspond to a gradual shift of the L↔M equilibrium in favor of the pure M state (i.e., the deprotonated Schiff base form). On the other hand, light-activated pHR follows a sequence in which bathochromically absorbing O_{600} is formed. The first transformation of this path (50 μs) occurs between two L_{520} chromophore states, which are spectrally identical and therefore constitute a typical spectrally silent transition. Note that the identity of the L_{520} spectra in P_2 and P_3 have been observed throughout all varied parameters. Interestingly, time-resolved Fourier transform infrared (FTIR) data of P_2 and P_3 display differences in a region characteristic for amide I/II vibration modes (1500–1700 cm^{-1}) (Hackmann et al., 2001). Obviously, the term spectrally silent is true only for distinct wavelength regions. It should be noted that low-temperature FTIR difference spectra of HR from *H. salinarum* revealed also two L photointermediates distinguished by their protein and water FTIR bands (Chon et al., 1999).

Only in the next step, P_4, does the O_{600} state start to appear. The absorption maximum at 600 nm indicates that chloride is not any longer in close proximity to the chromophore (Scharf and Engelhard, 1994). The previous steps are apparently an essential prerequisite of moving halide anions away from the binding site. The corresponding molecular mechanism of this process is very intriguing. According to the data of Gerscher et al. (1997) the halide anion established in the L state forms a stronger hydrogen bond with the protonated Schiff base than in the ground state. Presumably, this could lead to a lowering of the affinity to the original chloride-binding site in which Arg-123 might be involved (Rüdiger and Oesterhelt, 1997). Gerscher et al. (1997) suggested that the all-*trans*→13-*cis* isomerization of retinal that precedes the L formation may also move the halide ion closer to the cytoplasm channel. Which of the three steps ($P_1 \rightarrow P_2 \rightarrow P_3 \rightarrow P_4$) can be assigned to the displacement of the halide has still to be elucidated.

As discussed above, the curvature of the k_4 temperature dependence implies that the precursor of the $P_4 \rightarrow P_5$ transition has to be O^1_{600} and not L_{520}. It follows that the actual release of chloride from the Schiff base environment occurs during the lifetime of P_4 in a reversible reaction ($L_{520} \leftrightarrow O^1_{600}$). The vectorial transport can proceed because the subsequent $P_4 \rightarrow P_5$ transition is irreversible and might involve either a conformational change of the protein and/or the *cis-trans* isomerization of the retinal as rate-limiting step. The next kinetic state is again characterized by a fast equilibrium between O^2_{600} and N_{520}. The species absorbing at 520 nm has been assigned to an N-type intermediate although the spectroscopic properties are identical to those of L of the previous equilibrium (P_4). As outlined above, the O^1_{600} intermediate in P_4 represents a state in which the chloride ion is already released from its binding site toward the cytoplasm. On the other hand, the O^2_{600} intermediate in P_5 may be ready to pick up chloride from the extracellular side of pHR, thereby forming in a reversible reaction a species absorbing at 520 nm (S_2). Thus, the major difference between O^1_{600} in P_4 and O^2_{600} in P_5 is the accessibility toward the cytoplasm and the periplasm, respectively. In analogy to the BR photocycle and to principal considerations concerning the $M_1 \rightarrow M_2$ transition we assign the two different O-states in P_4 and P_5 to an $O^1_{600} \rightarrow O^2_{600}$ conversion. Because, according to the BR photocycle nomenclature, L and N intermediates are distinguished by the accessibility of the Schiff base toward the cytoplasmic and extracellular channels we define the S_2 state in P_5 as N.

It should be noted that this mechanism implies that the decay of P_5 occurs from N_{520} and not from O^2_{600}. However, this coupling cannot be unequivocally deduced from the measured data. For instance, if the $P_5 \rightarrow P_6$ transition occurs from the N_{520} state, then one would expect an acceleration of the k_5 rate constant about six times on increasing the chloride concentration from 150 mM to 2 M (see Fig. 6, inset; partitioning of N_{520} increases from 0.1 to 0.6). Experimentally, this rate is only two times accelerated (Fig. 3 *B*). Therefore, an unambiguous assignment is not possible.

The last transition of the photocycle, $P_5 \rightarrow$pHR, seems to be a minor rearrangement of the pHR molecule while all charges within the vicinity of the chromophore should already be more or less relaxed. One could speculate that this transition might be related to the final release of the halide

ion into the buffer on the cytoplasmic side and/or the uptake of the ion at the entrance port of the extracellular side.

Using the data presented in this paper the affinity changes during the photocycle can be estimated assuming a model with two halide anion-binding sites. These two sites A_1 and A_2 differ from each other by their location with respect to the retinal chromophore and their affinities toward halide anions. Whereas A_1 is located in the vicinity of the Schiff base and has access to the periplasm medium, A_2 is positioned, almost excluded from the bulk phase, within the cytoplasmic half of pHR. The binding of an anion to A_1 affects the chromophore ground spectrum, which is shifted from 600 nm in the halide-free form to 575 nm once a halide anion has bound. The binding to A_2 does not affect the chromophore ground spectrum. The binding constants of A_1 in the ground state ($pHR_{575} \leftrightarrow pHR_{600}$) are 2.5, 1, and 3 mM for Cl, Br, and I, respectively. During the photocycle similar spectral changes are established in P_4 ($L_{520} \leftrightarrow O^1_{600}$) and P_5 ($O^2_{600} \leftrightarrow N_{520}$) but with significantly different apparent affinities of anion binding. The P_4 equilibrium is not dependent on the concentration of chloride or on the replacement of Cl by Br or I but is sensitive toward changes of the temperature within the measured range of parameters. This implies the existence of a second anion-binding site A_2 that accepts an anion from the A_1. Both sites have sufficiently low affinities to be insensitive to the external concentration of halides in the P_4 state.

Contrary to P_4, the P_5 ($O^2_{600} \leftrightarrow N_{520}$) equilibrium is almost insensitive to the temperature at a chloride concentration of 150 mM but is highly sensitive to the concentration of Cl and to the type of anion at 20°C. Therefore, in the P_5 state the A_1 site is available to the external medium and has affinity constants of 1.1, 0.3, and 0.1 M for Cl, Br, and I, respectively. This is equivalent to the rise of the binding free energy of ~15, 14, and 9 kJ/mol at 20°C in comparison with the ground state. Assuming that after the $P_4 \rightarrow P_5$ step the affinity of the A_1 may slightly increase (or does not change at all) the lower limit for the A_2 affinity can be estimated as ~5.7 M for chloride in the P_4 state. For this calculation a free energy difference of 4 kJ/mol between A_1 and A_2 has been used as can be extracted from the temperature dependence of P_4.

The chloride replacement by bromide and iodide does not change the P_4 equilibrium but significantly increases the affinity of the A_1 in the P_5 state from 1.1 to 0.3 and 0.1 M, respectively. Similarly, the limit of the A_2 affinity is increased from 5.7 M (chloride) to 1.5 M and 0.5 M for bromide and iodide, respectively. This finding predicts that at concentrations of the halide anion above their binding constants the transport activity of pHR should be inhibited by a factor of more than two due to the occupancy of the A_2 binding site. Bamberg et al. (1984) experimentally observed this effect by measuring the electrogenicity of sHR in black lipid membranes. The steady-state photocurrent was significantly reduced when chloride was replaced by bromide or iodide already in the 100 mM range. Recently, Okuno et al. (1999) have measured the photoelectric response of the sHR and pHR toward a wide range (up to 12 M) of chloride concentrations. The authors obtained a bell-shaped dependence of the transport activity on the concentration of chloride, which provided an apparent affinity of the chloride release binding sites of 7.5 M for the sHR. In the case of pHR two affinities (0.2 M and 5.6 M) were obtained. The latter value is very close to the above estimation (5.7 M). However, the former data (0.2 M) cannot be reconciled with our photocycle experiments. In two other papers, Ludmann et al. (2000) and Kalaidzidis et al. (1998) have measured the photoelectric response of pHR in dependence of the chloride concentration. Both groups did not obtain any significant inhibition of the transport up to 2 M Cl. Thus, this additional 0.2 M affinity site might be due to the experimental conditions used by Okuno et al. (1999).

The concept of at least two halide-binding sites with a high-affinity site close to the retinal Schiff base and a low-affinity site within the ion-release channel was first proposed by Lanyi for sHR (Lanyi, 1984). Lanyi reasoned that the photo-isomerization of retinal causes an increase of the affinity of the second site, which permits the chloride to move away from the first site. According to our data the photo-excitation of the pHR leads to a significant decrease of the A_1 affinity (near the retinal) from 2.5 mM to 1.1 M but does not change the A_2 (ion-releasing channel) affinity. Moreover, this altered affinity does not seem to be a direct consequence of the photo-isomerization, because it occurs only after P_4 is reached. Thus, the model presented in this paper is topologically similar to the hypothesis of Lanyi, but it differs in the mechanism. It should be noted that Okuno et al. (1999) in their model proposed three halide-binding sites in sHR and pHR. The authors assumed that the key site B, which is located close to the chromophore, experiences upon photo-excitation a considerable decrease of its affinity. This is supported by our analysis.

It is interesting to compare our results on the halide anion substitution with data recently obtained on the permeation of halide anions (Cl, Br, and I) through phospholipid bilayers (Paula et al., 1998). The authors showed that the permeability coefficients for iodide and bromide are ~50 and 10 times higher than for chloride and conclude that the major physical parameter responsible for the differences is the dehydration free energy. It is the highest for chloride and decreases from bromide to iodide (~10 kJ/mol, 5 kJ/mol, and 0.5 kJ/mol, respectively). We obtained similar trends in the A_1 and A_2 affinities of the P_4 and P_5 kinetic states. The free energy differences are $RT \ln(1.1/0.3) \approx 3$ kJ/mol between chloride and bromide and $RT \ln(1.1/0.1) \approx 6$ kJ/mol between chloride and iodide at $T = 293$ K. On the other hand, the A_1 affinity in the unphotolyzed state of pHR does not show this systematic tendency (2.5 mM, 1 mM, and 3 mM for Cl, Br, and I, respectively). This result indicates that in the metastable energization of halides in the P_4 and P_5

states the interaction of ions with dielectrically unrelaxed protein environment near the A_1 site plays a significant role. Whereas in the ground state the protein (and probably water molecules) provides a sufficient compensation for the hydration shell, other effects affecting the affinity of the A_1 seem to dominate. On the other hand, the affinity of the A_2-binding site does not alter upon photoexcitation but shows the same dependency on the dehydration energy. This implies that protein environment of this site has the dielectric constant similar to the lipid and/or should not contain positive polar groups.

The proposed kinetic model differs partly from pHR (and sHR) photocycle models recently discussed in the literature (Ludmann et al., 2000; Váró et al., 1995a,b,c). The main difference concerns the assumption that the observed rate constants are not the products (more exactly the Eigen values) of many microscopic (or intrinsic) reversible transitions between intermediates but that they are themselves the microscopic irreversible transitions between kinetically resolved states of a single relaxation chain. This postulation greatly simplifies the task of data evaluation because the model has no free parameters and therefore does not suffer from the global minimum problem. As a reward, this simplest among other possible models provides a quite reasonable description of the complex kinetic process. Until there are no strong experimental evidences that contradict this model one should follow the good advice of the English philosopher William of Ockham (1285–1349): "Pluralitas non est ponenda sine neccesitate" or, in one of the modern versions: "Always choose the simplest hypothesis that explains the data at hand."

CONCLUSIONS

The pHR photocycle describes a relatively simpler relaxation pathway than those of BR or pSRII. After the K intermediate it contains only six kinetic and three spectral states versus eight kinetic and five spectral states of the BR and pSRII. Experimentally, these properties led to significantly higher spectral resolution of the intermediates. Their photocycle dependence on temperature, concentration of halide anions, and the type of halides led to establish the thermodynamics of the halide transport. The key step in the halide transport across the membrane occurs during the transition of P_4 to P_5, which concomitantly represents a switch between two different O-spectral states. In analogy to the BR photocycle this switch can be compared with the $M_1 \rightarrow M_2$ transition, which changes the access from the extracellular channel to the cytoplasmic channel. In contrast, in the pHR $O_1 \rightarrow O_2$ transition, the accessibility is changed from the cytoplasmic to the extracellular channel. It might be worthwhile to study the pH and temperature dependence of the BR photocycle in greater detail that might provide further insight into the still controversial kinetics of M-formation and M-decay.

It should be emphasized that the data have been analyzed by assuming a stringent model of irreversible reactions. It is therefore appropriate to cite Alon et al. (1998) on the relationship between data and model: "Fitting data to a model does not constitute a validation of the model's assumptions. We hope, however, that this model can serve as a simple basis for comparison for future experiments that could shed light on the switch mechanism."

We thank R. Müller, K.-H. Müller, H. Schlüter, and J. Hüber for excellent technical help and A. A. Wegener for *E. coli* expressed pHR. B. Hess and D. S. Chernavskii are acknowledged for their long term support and motivation. We thank D. Oesterheld for a fruitful discussion on the O^1-O^2 switch.

This work was supported by a grant (EN 87/10–2) from the Deutsche Forschungsgemeinschaft.

REFERENCES

Alon, U., L. Camarena, M. G. Surette, B. A. Y. Arcas, Y. Liu, S. Leibler, and J. B. Stock. 1998. Response regulator output in bacterial chemotaxis. *EMBO J.* 17:4238–4248.

Ames, J. B., J. Raap, J. Lugtenburg, and R. A. Mathies. 1992. Resonance Raman study of halorhodopsin photocycle kinetics, chromophore structure, and chloride-pumping mechanism. *Biochemistry.* 31:12546–12554.

Bamberg, E., P. Hegemann, and D. Oesterhelt. 1984. Reconstitution of the light-driven electrogenic ion pump halorhodopsin in black lipid membranes. *Biochim. Biophys. Acta.* 773:53–60.

Bamberg, E., J. Tittor, and D. Oesterhelt. 1993. Light-driven proton or chloride pumping by halorhodopsin. *Proc. Natl. Acad. Sci. U.S.A.* 90: 639–643.

Birge, R. R. 1990. Nature of the primary photochemical events in rhodopsin and bacteriorhodopsin. *Biochim. Biophys. Acta.* 1016:293–327.

Bivin, D. B., and W. Stoeckenius. 1986. Photoactive retinal pigments in haloalkaliphilic bacteria. *J. Gen. Microbiol.* 132:2167–2177.

Blanck, A., and D. Oesterhelt. 1987. The halo-opsin gene. II. Sequence, primary structure of halorhodopsin and comparison with bacteriorhodopsin. *EMBO J.* 6:265–273.

Chizhov, I., D. S. Chernavskii, M. Engelhard, K. H. Müller, B. V. Zubov, and B. Hess. 1996. Spectrally silent transitions in the bacteriorhodopsin photocycle. *Biophys. J.* 71:2329–2345.

Chizhov, I., G. Schmies, R. Seidel, J. R. Sydor, B. Lüttenberg, and M. Engelhard. 1998. The photophobic receptor from *Natronobacterium pharaonis*: temperature and pH dependencies of the photocycle of sensory rhodopsin II. *Biophys. J.* 75:999–1009.

Chon, Y. S., H. Kandori, J. Sasaki, J. K. Lanyi, R. Needleman, and A. Maeda. 1999. Existence of two L photointermediates of halorhodopsin from *Halobacterium salinarum*, differing in their protein and water FTIR bands. *Biochemistry.* 38:9449–9455.

Duschl, A., J. K. Lanyi, and L. Zimányi. 1990. Properties and photochemistry of a halorhodopsin from the haloalkalophile *Natronobacterium pharaonis. J. Biol. Chem.* 265:1261–1267.

Gerscher, S., M. Mylrajan, P. Hildebrandt, M. H. Baron, R. Müller, and M. Engelhard. 1997. Chromophore-anion interactions in halorhodopsin from *Natronobacterium pharaonis* probed by time-resolved resonance Raman spectroscopy. *Biochemistry.* 36:11012–11020.

Hackmann, C., J. Guijarro, I. Chizhov, M. Engelhard, C. Rödig, and F. Siebert. 2001. Static and time-resolved step-scan FTIR investigations of the photoreaction of halorhodopsin from *Natronobacterium pharaonis*: consequences for models of the anion translocation mechanism. *Biophys. J.* 81:394–406.

Hartmann, R., and D. Oesterhelt. 1977. Bacteriorhodopsin-mediated photophosphorylation in *Halobacterium halobium. Eur. J. Biochem.* 77: 325–335.

Haupts, U., J. Tittor, E. Bamberg, and D. Oesterhelt. 1997. General concept for ion translocation by halobacterial retinal proteins: the isomerization/switch/transfer (IST) model. *Biochemistry.* 36:2–7.

Havelka, W. A., R. Henderson, J. A. W. Heymann, and D. Oesterhelt. 1993. Projection structure of halorhodopsin from *Halobacterium halobium* at 6 Å resolution obtained by electron cryo-microscopy. *J. Mol. Biol.* 234:837–846.

Hegemann, P., D. Oesterhelt, and M. Steiner. 1985. The photocycle of the chloride pump halorhodopsin. I. Azide-catalyzed deprotonation of the chromophore is a side reaction of photocycle intermediates inactivating the pump. *EMBO J.* 4:2347–2350.

Heyde, M. E., D. Gill, R. G. Kilponen, and L. Rimai. 1971. Raman spectra of Schiff bases of retinal (models of visual photoreceptors). *J. Am. Chem. Soc.* 93:6776–6780.

Hoff, W. D., K. H. Jung, and J. L. Spudich. 1997. Molecular mechanism of photosignaling by archaeal sensory rhodopsins. *Annu. Rev. Biophys. Biomol. Struct.* 26:223–258.

Kalaidzidis, I. V., Y. L. Kalaidzidis, and A. D. Kaulen. 1998. Flash-induced voltage changes in halorhodopsin from *Natronobacterium pharaonis*. *FEBS Lett.* 427:59–63.

Kolbe, M., H. Besir, L. O. Essen, and D. Oesterhelt. 2000. Structure of the light-driven chloride pump halorhodopsin at 1.8 Ångstrom resolution. *Science.* 288:1390–1396.

Lanyi, J. K. 1984. Light-dependent *trans* to *cis* isomerization of the retinal in halorhodopsin. *FEBS Lett.* 175:337–342.

Lanyi, J. K. 1999. Progress toward an explicit mechanistic model for the light-driven pump, bacteriorhodopsin. *FEBS Lett.* 464:103–107.

Lanyi, J. K., A. Duschl, G. W. Hatfield, K. May, and D. Oesterhelt. 1990. The primary structure of a halorhodopsin from *Natronobacterium pharaonis*: structural, functional and evolutionary implications for bacterial rhodopsins and halorhodopsins. *J. Biol. Chem.* 265:1253–1260.

Lanyi, J. K., and G. Váró. 1995. The photocycles of bacteriorhodopsin. *Isr. J. Chem.* 35:365–385.

Lanyi, J. K., and V. Vodyanoy. 1986. Flash spectroscopic studies of the kinetics of the halorhodopsin photocycle. *Biochemistry.* 25:1465–1470.

Ludmann, K., G. Ibron, J. K. Lanyi, and G. Váró. 2000. Charge motions during the photocycle of pharaonis halorhodopsin. *Biophys. J.* 78: 959–966.

Matsuno-Yagi, A., and Y. Mukohata. 1980. ATP synthesis linked to light-dependent proton uptake in a rad mutant strain of *Halobacterium* lacking bacteriorhodopsin. *Arch. Biochem. Biophys.* 199:297–303.

Michel, H., and D. Oesterhelt. 1980. Electrochemical proton gradient across the cell membrane of *Halobacterium halobium*: effect of *N,N′*-dicyclohexylcarbodiimide, relation to intracellular adenosine triphosphate, adenosine diphosphate, and phosphate concentration, and influence of the potassium gradient. *Biochemistry.* 19:4607–4614.

Muneyuki, E., C. Shibazaki, H. Ohtani, D. Okuno, M. Asaumi, and T. Mogi. 1999. Time-resolved measurements of photovoltage generation by bacteriorhodopsin and halorhodopsin adsorbed on a thin polymer film. *J. Biochem. (Tokyo).* 125:270–276.

Müller, K.-H., H. J. Butt, E. Bamberg, K. Fendler, B. Hess, F. Siebert, and M. Engelhard. 1991. The reaction cycle of bacteriorhodopsin: an analysis using visible absorption, photocurrent and infrared techniques. *Eur. Biophys. J.* 19:241–251.

Müller, K.-H., and T. Plesser. 1991. Variance reduction by simultaneous multi-exponential analysis of data sets from different experiments. *Eur. Biophys. J.* 19:231–240.

Oesterhelt, D. 1995. Structure and function of halorhodopsin. *Isr. J. Chem.* 35:475–494.

Oesterhelt, D., P. Hegemann, and J. Tittor. 1985. The photocycle of the chloride pump halorhodopsin. II. Quantum yields and a kinetic model. *EMBO J.* 4:2351–2356.

Okuno, D., M. Asaumi, and E. Muneyuki. 1999. Chloride concentration dependency of the electrogenic activity of halorhodopsin. *Biochemistry.* 38:5422–5429.

Paula, S., A. G. Volkov, and D. W. Deamer. 1998. Permeation of halide anions through phospholipid bilayers occurs by the solubility-diffusion mechanism. *Biophys. J.* 74:319–327.

Rüdiger, M., and D. Oesterhelt. 1997. Specific arginine and threonine residues control anion binding and transport in the light-driven chloride pump halorhodopsin. *EMBO J.* 16:3813–3821.

Sasaki, J., L. S. Brown, Y.-S. Chon, H. Kandori, A. Maeda, R. Needleman, and J. K. Lanyi. 1995. Conversion of bacteriorhodopsin into a chloride ion pump. *Science.* 269:73–75.

Schäfer, G., M. Engelhard, and V. Müller. 1999. Bioenergetics of the archaea. *Microbiol. Mol. Biol. Rev.* 63:570–620.

Scharf, B., and M. Engelhard. 1994. Blue halorhodopsin from *Natronobacterium pharaonis*: wavelength regulation by anions. *Biochemistry.* 33: 6387–6393.

Schobert, B. and J. K. Lanyi. 1982. Halorhodopsin is a light-driven chloride pump. *J. Biol. Chem.* 257:10306–10313.

Taylor, M. E., R. A. Bogomolni, and H. J. Weber. 1983. Purification of photochemically active halorhodopsin. *Proc. Natl. Acad. Sci. U.S.A.* 80:6172–6176.

Tittor, J., D. Oesterhelt, R. Maurer, H. Desel, and R. Uhl. 1987. The photochemical cycle of halorhodopsin: absolute spectra of intermediates obtained by flash photolysis and fast difference spectra measurements. *Biophys. J.* 52:999–1006.

Tsuda, M., N. Hazemoto, M. Kondo, N. Kamo, Y. Kobatake, and Y. Terayama. 1982. Two photocycles in *Halobacterium halobium* that lacks bacteriorhodopsin. *Biochem. Biophys. Res. Commun.* 108: 970–976.

Váró, G., L. S. Brown, J. Sasaki, H. Kandori, A. Maeda, R. Needleman, and J. K. Lanyi. 1995b. Light-driven chloride ion transport by halorhodopsin from *Natronobacterium pharaonis*. I. The photochemical cycle. *Biochemistry.* 34:14490–14499.

Váró, G., R. Needleman, and J. K. Lanyi. 1995c. Light-driven chloride ion transport by halorhodopsin from *Natronobacterium pharaonis*. II. Chloride release and uptake, protein conformation change, and thermodynamics. *Biochemistry.* 34:14500–14507.

Váró, G., L. Zimányi, X. Fan, L. Sun, R. Needleman, and J. K. Lanyi. 1995a. Photocycle of halorhodopsin from *Halobacterium salinarium. Biophys. J.* 68:2062–2072.

Wittenberg, R. Charakterisierung der Elektronentransportkette und Untersuchungen zur Bioenergetik in *Natronobacterium pharaonis*. 1995. Ph.D. thesis. Ruhr-Universität, Bochum, Germany. 101 pp.

Zimányi, L., L. Keszthelyi, and J. K. Lanyi. 1989. Transient spectroscopy of bacterial rhodopsins with an optical multichannel analyzer. I. Comparison of the photocycles of bacteriorhodopsin and halorhodopsin. *Biochemistry.* 28:5165–5172.

Zimányi, L., and J. K. Lanyi. 1997. Fourier transform Raman study of retinal isomeric composition and equilibration in halorhodopsin. *J. Phys. Chem. B.* 101:1930–1933.